Microglia depletion exacerbates demyelination and impairs remyelination in a neurotropic coronavirus infection

Alan Sariol[a], Samantha Mackin[b], Merri-Grace Allred[a], Chen Ma[c], Yu Zhou[c], Qinran Zhang[c], Xiufen Zou[c], Juan E. Abrahante[d], David K. Meyerholz[e], and Stanley Perlman[a,b,1]

[a]Interdisciplinary Program in Immunology, University of Iowa, Iowa City, IA 52242; [b]Department of Microbiology and Immunology, University of Iowa, Iowa City, IA 52242; [c]School of Mathematics and Statistics, Wuhan University, 430072 Wuhan, China; [d]University of Minnesota Informatics Institute (UMII), Minneapolis, MN 55455; and [e]Department of Pathology, University of Iowa, Iowa City, IA 52242

Edited by Lawrence Steinman, Stanford University School of Medicine, Stanford, CA, and approved July 17, 2020 (received for review April 22, 2020)

Microglia are considered both pathogenic and protective during recovery from demyelination, but their precise role remains ill defined. Here, using an inhibitor of colony stimulating factor 1 receptor (CSF1R), PLX5622, and mice infected with a neurotropic coronavirus (mouse hepatitis virus [MHV], strain JHMV), we show that depletion of microglia during the time of JHMV clearance resulted in impaired myelin repair and prolonged clinical disease without affecting the kinetics of virus clearance. Microglia were required only during the early stages of remyelination. Notably, large deposits of extracellular vesiculated myelin and cellular debris were detected in the spinal cords of PLX5622-treated and not control mice, which correlated with decreased numbers of oligodendrocytes in demyelinating lesions in drug-treated mice. Furthermore, gene expression analyses demonstrated differential expression of genes involved in myelin debris clearance, lipid and cholesterol recycling, and promotion of oligodendrocyte function. The results also demonstrate that microglial functions affected by depletion could not be compensated by infiltrating macrophages. Together, these results demonstrate that microglia play key roles in debris clearance and in the initiation of remyelination following infection with a neurotropic coronavirus but are not necessary during later stages of remyelination.

microglia | virus-induced demyelination | coronavirus | neuroinflammation | remyelination

Viral infections of the CNS require a delicate balance of pro- and anti-inflammatory factors in order to clear infection while causing minimal immunopathology. A variety of human CNS viral infections, including those caused by JC virus, HHV6, HTLV-1, and measles virus, are known to result in demyelinating diseases (1–4). Viral infection, among other environmental factors, is also thought to be involved in the etiology and recrudescence of multiple sclerosis (MS) (5–8), an autoimmune demyelinating disease of the CNS.

Microglia are the yolk sac-derived resident macrophages of the CNS parenchyma (9). While these cells play an important role in maintaining CNS homeostasis, they are additionally known to play critical roles surveilling the CNS, allowing for detection of pathological events (10–12). As myeloid cells, they are known to engage in antigen presentation, secrete pro- and anti-inflammatory cytokines and chemokines, phagocytose pathogens, as well as cellular debris (13–15). Dysfunctional microglia, however, have been observed to contribute to a variety of neurodegenerative disorders in the CNS (16). In the context of autoimmune and chemically induced demyelinating diseases, such as experimental autoimmune encephalomyelitis (EAE) and MS, microglia are thought to play disparate roles (17). Microglia are present and highly activated in lesions of demyelination where they have been described to have both harmful roles, such as production of cytotoxic cytokines, contribution to oxidative damage, and promotion of pathogenic T cell responses, as well as beneficial roles, including promotion of oligodendrocyte differentiation and clearance of myelin and cellular debris (14, 17–19). Because microglia are the primary immune sentinels of the CNS parenchyma (12), they are uniquely positioned to respond to viral infection and contribute to the immune-mediated events that follow.

Neurotropic coronaviruses, such as the JHMV strain of MHV, cause acute and chronic demyelinating encephalomyelitis (20). MHV, a betacoronavirus, is related to SARS-CoV, MERS-CoV, and SARS-CoV-2, the newly identified cause of pandemic pneumonia (21). Following infection with the neuroattenuated rJ2.2 variant of JHMV (called JHMV herein) (22), mice develop mild acute encephalitis around 5–10 d postinfection (dpi), which 80–90% of mice survive. Surviving mice go on to develop immune-mediated demyelination and hind-limb paresis/paralysis as a consequence of viral clearance, beginning 7 to 8 dpi and peaking at 12–14 dpi. These mice, then, begin to recover from demyelination and undergo remyelination as the antiviral immune response resolves. Microglia are known to be activated following JHMV infection and play a critical role in the early immune response to the virus; in their absence during the first 3 d of infection, mice uniformly succumb to the infection (23). However, little is known regarding their role in recovery from demyelination that follows. It is known that microglia along with blood-borne infiltrating macrophages are present and activated within lesions of MHV-induced demyelination and that depletion

Significance

Microglia are the resident phagocytic cells of the central nervous system (CNS). During demyelination, a condition in which myelin sheaths are damaged and removed from neurons due to inflammation, microglia can play both harmful and beneficial roles, but their exact functions are still unclear. Using a drug that depletes microglia, we demonstrate that, after infection with JHMV, a coronavirus that infects the CNS of rodents and causes immune-mediated demyelination, microglia are essential for repair following demyelination. We found that microglia played critical roles in initiating this repair process by clearing myelin debris and producing prorepair factors, both of which promote the presence and the function of oligodendrocytes, the cells responsible for repairing and replacing myelin sheaths within areas of damage.

Author contributions: A.S. and S.P. designed research; A.S., S.M., and M.-G.A. performed research; A.S., C.M., Y.Z., Q.Z., X.Z., J.E.A., D.K.M., and S.P. analyzed data; and A.S. and S.P. wrote the paper.

The authors declare no competing interest.

This article is a PNAS Direct Submission.

[1]To whom correspondence may be addressed. Email: stanley-perlman@uiowa.edu.

This article contains supporting information online at https://www.pnas.org/lookup/suppl/doi:10.1073/pnas.2007814117/-/DCSupplemental.

First published September 14, 2020.

of those peripheral macrophages does not alter demyelination (24, 25); however, whether microglia play a pathogenic or protective role following demyelinating encephalomyelitis is largely unknown.

To better understand the role that microglia play in virus-induced demyelination and subsequent remyelination, we treated mice with PLX5622, an inhibitor of CSF1R tyrosine-kinase activity, which results in microglia depletion (23, 26). Depletion of microglia at the peak of the adaptive immune response to JHMV allowed mice to clear the virus and survive the acute encephalitis, while also allowing for study of the role of microglia in the demyelination and subsequent remyelination that follows these early events. Here, we show that microglia are critical for the resolution of demyelination and initiation of remyelination and recovery following JHMV infection. Mice in which microglia were depleted in the later stages of virus clearance failed to recover clinically from hind-limb paralysis and or resolve lesions of demyelination. However, delayed PLX5622 treatment indicated that microglia function was most critical in the early stages of remyelination but was dispensable at later times in the remyelination process.

Results

Depletion of Microglia after Viral Clearance Exacerbates Disease. To assess the role of microglia in the processes of demyelination and remyelination that follow JHMV clearance, we infected mice intracranially with 700 plaque forming units (PFUs) of JHMV. We, then, treated them beginning at 7 dpi with dietary PLX5622, which results in depletion of microglia but not monocyte-derived macrophages if provided to naive animals or prior to infection

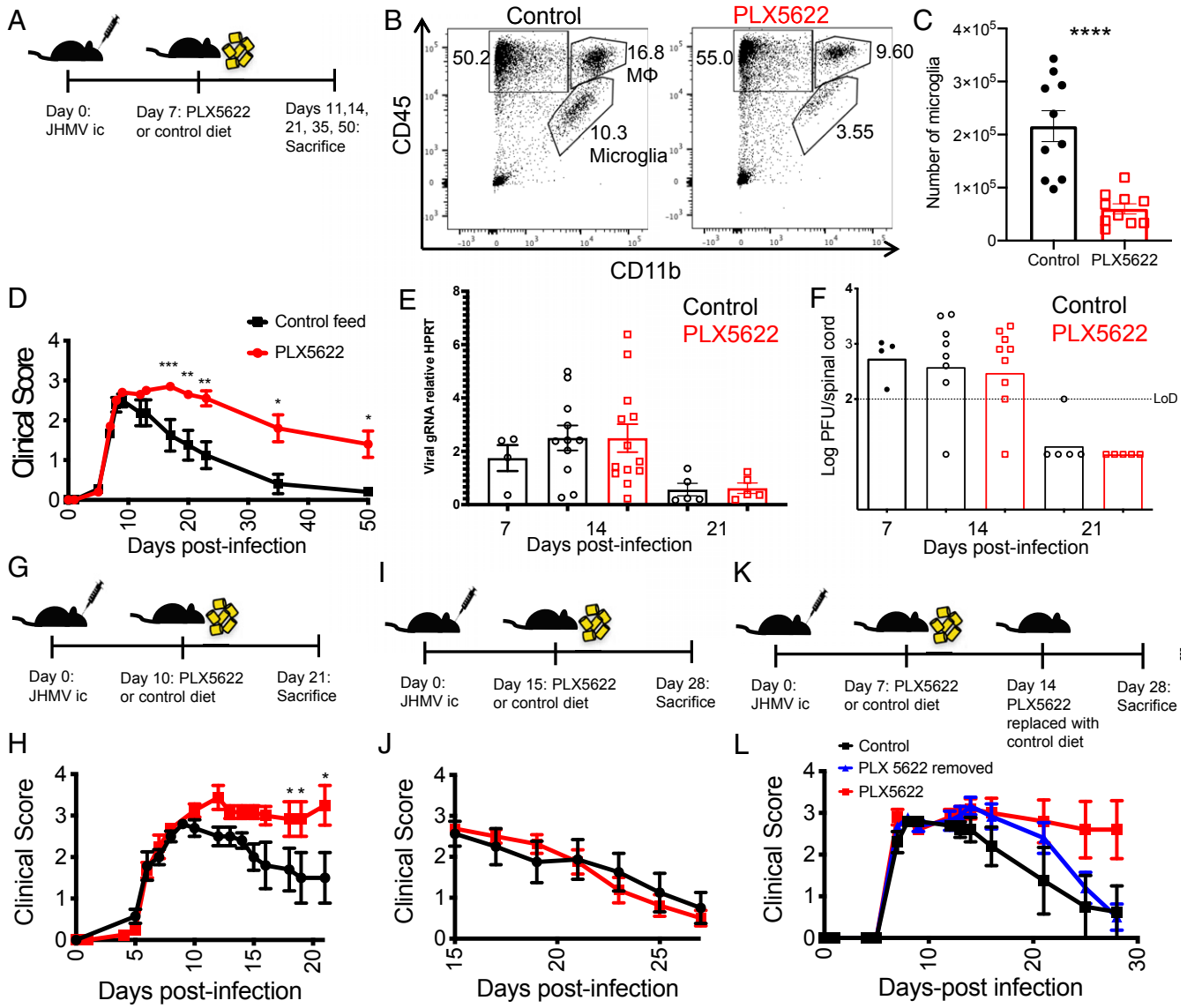

Fig. 1. Exacerbated disease in mice depleted of microglia. Mice were infected intracranially with 700-PFU JHMV, then fed at day 7 p.i. with PLX5622-containing or control chow (*A–F*). Representative flow plots of spinal cords showing gating for lymphocytes ($CD45^{+}CD11b^{-}$), monocytes/macrophages ($CD45^{hi}CD11b^{+}$, MΦ), and microglia ($CD45^{int}CD11b^{+}$) at day 14 p.i. (*B*). Summary of numbers of microglia in spinal cords at day 14 p.i. (*C*). Clinical scores at indicated days p.i. (*D*). (*B–D* $n = 10$ mice/group). Expression levels of viral genomic RNA (gRNA) as assessed by qPCR (*E*) ($n = 4–13$ mice/group) and infectious virus titers as determined by plaque assay in the spinal cord (*F*) ($n = 4–9$ mice/group). Mice were infected and fed at day 10 (*G* and *H*) or day 15 (*I* and *J*) p.i. with PLX5622-containing or control chow. Mice were infected and fed PLX5622-containing or control chow at day 7, followed by replacement of PLX5622-containing chow with control chow at 14 dpi (*K* and *L*). Clinical scores at indicated days p.i. (*H*, *J*, and *L*) ($n = 5–10$ mice/group). Data represent the mean ± SEM, $*P < 0.05$, $**P < 0.01$, $***P < 0.001$, $****P < 0.0001$ by Mann–Whitney *U* test.

(26, 27). Drug was added at 7 dpi (Fig. 1*A*) because microglia are critical for virus clearance in the first few days after infection (23). JHMV is largely cleared from the brain by 7 dpi (*SI Appendix*, Fig. S1) (20). At day 14 postinfection (p.i.), 7 d following the administration of PLX5622, microglia ($CD45^{int}CD11b^{+}$) were depleted by 70–75% in spinal cords compared to control diet-treated mice as assessed by flow cytometry (Fig. 1 *B* and *C*).

While mice that underwent microglia depletion reached the same peak clinical scores as mice treated with a control diet, these mice failed to undergo the recovery from clinical disease seen in control mice beginning at day 9–12, the time of peak disease (Fig. 1*D*). Mice lacking microglia continued to show signs of hind-limb weakness or paralysis through day 50 and beyond, while control mice were mostly fully recovered by 35 dpi. While infectious virus was cleared from the brain by 11 dpi (*SI Appendix*, Fig. S1), clearance from the spinal cord was incomplete by 14 dpi (Fig. 1*F*). To assess the effects of drug treatment on viral clearance, we next assessed viral titers in control- and PLX5622-treated mice. We observed no substantial differences in viral genomic material or in infectious virus as measured by plaque assay between control- and PLX5622-treated mice at 14 or 21 dpi in the spinal cord or brain (Fig. 1 *E* and *F* and *SI Appendix*, Fig. S1). Infectious virus was fully cleared by 21 dpi in both brain and spinal cord, while levels of gRNA were greatly decreased. Together, these results demonstrate a critical role for microglia in recovery from clinical disease that is independent of virus clearance and that virus clearance is able to proceed in the absence of microglia following the initiation of the adaptive immune response.

These data demonstrating impairments in recovery after PLX5622 treatment suggested that microglia played a role in the initiation of this process, so we next sought to identify the temporal window in which microglia perform this role. Delaying initiation of treatment with PLX5622 to 10 dpi (Fig. 1*G*) resulted in clinical scores similar to those observed in mice treated at 7 dpi (Fig. 1*H*). However, when depletion of microglia was delayed until 15 dpi (Fig. 1*I*), clinical signs of hind-limb paralysis were no different from control mice (Fig. 1*J*), suggesting that there is a limited window following the onset of demyelination in which microglia are critical for mitigating disease, following which they are dispensable. Withdrawal of PLX5622 treatment is known to result in a rapid and robust repopulation of microglia via self-renewal (28, 29), so we next provided PLX5622 at 7 dpi and, subsequently, removed the drug and replaced it with control feed at 14 dpi in order to determine whether microglia could perform their role in mitigating disease after delaying their presence (Fig. 1*K*). Following initially exacerbated disease while on PLX5622 treatment, these mice ultimately recovered similar to control-treated mice (Fig. 1*L*), suggesting that microglia are critical for the initiation of disease recovery rather than at a specific time after disease onset.

Mice Lacking Microglia Have Exacerbated Demyelination and Fail to Recover. The prolonged presence of hind-limb paralysis suggested that myelin destruction was ongoing or that remyelination was impaired. To begin to evaluate these possibilities, we next determined the impact of microglia depletion on the extent of demyelination in the spinal cord after Luxol fast blue (LFB) staining. Demyelination was present throughout the spinal cord especially in the cervical region at day 14 dpi. Modestly more myelin destruction was detected in PLX5622 compared to control-treated mice at day 14 dpi, but these differences were not statistically significant. By day 21, a time point at which control mice have begun to recover both clinically and histologically, we found that demyelination in the spinal cords of mice lacking microglia was unchanged while it had decreased substantially in controls (Fig. 2 *A* and *B*). By 50 dpi, a time point at which most control mice have fully recovered from clinical signs of disease, PLX5622-treated mice underwent little to no recovery in terms of demyelination with lesion sizes comparable to those at 21 dpi (Fig. 2 *A* and *C*). Furthermore, when we assessed mice treated with PLX5622 beginning at 15 dpi, which did not affect clinical disease (Fig. 1*J*), we observed no differences in the degree of demyelination in control- and PLX5622-treated mice when

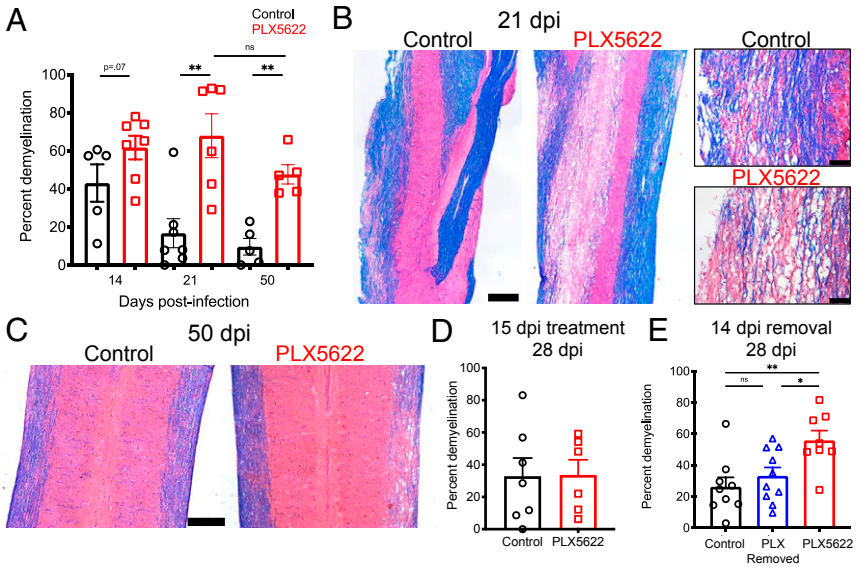

Fig. 2. Prolonged and exacerbated demyelination following microglia depletion. Mice were infected and fed with PLX5622-containing or control chow starting at day 7 p.i. Demyelination was quantified at indicated times p.i. (*A*). Representative images of LFB and hematoxylin and eosin (H&E) stained thoracic spinal cords at day 21 (*B*) and cervical spinal cords at day 50 (*C*) p.i. Mice were infected and fed at day 15 p.i. with PLX5622-containing or control chow and demyelination quantified at day 28 p.i. (*D*). Mice were infected and fed PLX5622-containing or control chow at day 7, followed by replacement of PLX5622-containing chow with control chow at 14 dpi, and demyelination was quantified at day 28 p.i. (*E*). (Scale bars, 500 μm.) Except for two images on the right hand side of panel *B* where scale bar, 100 μm. Data shown in *A* are representative of two independent experiments with 5–7 mice per group. Data represent the mean ± SEM, $*P < 0.05$, $**P < 0.01$ by Mann–Whitney *U* test.

assessed at 28 dpi (Fig. 2*D*) further reinforcing the notion that microglia are essential for initiating steps leading to reduced demyelination and increased remyelination. In addition, treatment with PLX5622 at 7 dpi and subsequent replacement with control chow at 14 dpi (Fig. 1 *K* and *L*) resulted in comparable levels of demyelination to mice receiving control chow and significantly less myelin destruction relative to mice that remained on PLX5622-containing chow when assessed at 28 dpi (Fig. 2*E*). Together, these data reinforced the notion that microglia are critical for the initiation of recovery from demyelination and that this process does not need to occur at a fixed time after infection.

Reduced Populations of Immune Cell Effectors Following Depletion of Microglia. The increased severity of demyelination in PLX5622-treated mice suggested a potential exacerbation of the inflammatory response, which could continue the process of immune-mediated demyelination and impair recovery (30–32). To assess the role of microglia in regulating the immune response following viral clearance, we first measured the numbers and frequency of infiltrating monocytes/macrophages ($CD45^{hi}CD11b^{+}Ly6G^{-}$) in the spinal cord at 14 dpi, 7 d after the onset of PLX5622 treatment. In mice depleted of microglia, monocytes/macrophages were reduced in both frequency and number compared to control mice (Fig. 3*A*). Furthermore, we observed an increase in the relative expression of Ly6C on these cells, suggesting a potential impairment in differentiation from inflammatory monocytes to mature macrophages. Of note, MHCI and MHCII expressions on macrophages were unaltered in the presence of PLX5622 treatment (Fig. 3*B*). Next, we measured the CD4 and CD8 T cell responses during demyelination as these cells play nonredundant roles as effectors of demyelination following JHMV infection (30). In the absence of microglia, we found decreases in the number of CD4 T cells (Fig. 3*C*), although the frequency of CD4 T cells specific for epitope M133, the immunodominant CD4 epitope (33), was the same as in control mice (Fig. 3 *D* and *E*). However, total numbers of M133-specific T cells were reduced in the drug-treated mice (Fig. 3*E*). Additionally, the number of $Foxp3^{+}$ Tregs was also diminished in mice lacking microglia, reflecting an overall reduction in the numbers of CD4 T cells (Fig. 3*F*). CD8 T cells were similarly decreased in terms of total numbers (Fig. 3*G*), although an increased frequency (but not number) was virus specific as measured by the response to the immunodominant CD8 T epitope (S510) of JHMV (Fig. 3 *H* and *I*) (34, 35). These data, which indicate that the depletion of microglia results in a reduction in the total and virus-specific T and myeloid cell immune responses, were unexpected because these cells are required for demyelination (25, 30).

Microglia Up-Regulate Factors Involved in Remyelination Following Viral Clearance. This decreased number of immune cells suggested, instead, that microglia played an important role in remyelination. To better understand the role of microglia in myelin repair, we isolated microglia from spinal cords of JHMV-infected mice at 14 dpi, corresponding with the peak of demyelination, onset of recovery, 21 dpi, a time when recovery and remyelination had substantially occurred, and from mock-infected mice. PLX5622-treated mice were not included in this experiment because microglia numbers were very low in these mice. We, then, performed next-generation RNA sequencing (RNA-seq) on these microglia to compare their transcriptomes and identified 1,818 total unique differentially expressed genes among the three pairwise group comparisons with 1,413 differentially regulated genes between microglia from mock-infected mice and mice at 14 dpi, 1,266 genes between mock and 21-dpi microglia, and 91 between 14- and 21-dpi animals. Most of the latter differences represented genes returning to mock-infected levels by day 21 p.i. (Fig. 4*A*). Several genes proposed to be involved in promoting remyelination were found to be generally up-regulated at both 14 and 21 dpi relative to mock-infected mice (Fig. 4*B*). Some of these genes encode for proteins that are purported to play a role in promoting oligodendrocyte maturation and proliferation, such as *Igf1* and *Lgals3* (Galectin 3) (36–39). Unexpectedly, *Cxcl12*, which is involved in remyelination (40), was down-regulated following infection. Furthermore, microglia at both 14 and 21 dpi up-regulated genes critical for the uptake and degradation of cellular and myelin debris, such as *Apoe*, *Clec7a*, and *Axl* (41–43). Accumulation of debris within lesions has been demonstrated to inhibit oligodendrocyte recruitment and differentiation (18, 41, 44) and, thus, delay recovery/remyelination. To confirm these results, we performed qPCR analyses for several of these genes using isolated microglia. As shown in Fig. 4*D*, we confirmed the up-regulation of *IGF1*, *Axl*, *ApoE*, *Tgm2*, *Lgals3*, and *Itgax* (CD11c) mRNA and the down-regulation of *CXCL12* mRNA at 14 dpi compared to mock-infected cells (Fig. 4*C*).

While microglia were depleted in mice treated with PLX5622, it is possible that infiltrating monocytes/macrophages compensated for some functions of microglia. To examine this possibility, we first focused on a single gene *Igf1*, which was up-regulated in our transcriptome study and is well described as important in both developmental myelination and remyelination (36, 37). In the CNS, IGF1 is primarily expressed by $CD11c^{+}$ microglia (37); however, in other tissues, $CD11c^{+}$ macrophages express IGF1 (45). We found that the gene encoding for CD11c (*Itgax*) was up-regulated by microglia at both 14 and 21 dpi (Fig. 4*B*). When isolated monocytes/macrophages ($CD45^{hi}CD11b^{+}Ly6G^{-}$) from PLX5622-treated and control mice were analyzed for *Igf1* mRNA and CD11c expression, we found a reduction in relative CD11c expression in PLX5622-treated mice (Fig. 4*D*) when assessed by flow cytometry but no significant difference in *Igf1* mRNA expression when assessed on a per cell basis (Fig. 4*C*). Analysis of mRNA levels of other purported promyelination genes identified in our RNA sequencing analyses in isolated monocytes/macrophages revealed no differential expression of these genes between control- and PLX5622-treated mice (Fig. 4*C*). Based on gene expression patterns in microglia after infection, we expected to find a decrease in the genes described above following microglia depletion. When whole spinal cords were analyzed, we observed statistically significant differences in *Igf1* and *Clec7a* messenger RNA (mRNA) expression and trends toward decreased expression in ApoE and Axl (*SI Appendix*, Fig. S2). Collectively, these data indicated that macrophages in drug-treated mice were unable to compensate for these promyelination functions in the absence of microglia, recognizing that some of this inability may stem from the decreased numbers of macrophages present in drug-treated spinal cords.

Increased Cellular Debris in Lesions of Mice Lacking Microglia. The transcriptome analyses identified potential roles for microglia in myelin and cellular debris removal and in myelin synthesis. Furthermore, the data in Fig. 2*B* suggest that more vacuolization occurs in PLX5622-treated compared to control mice, indicative of extensive white matter (WM) destruction. In order to assess the effects of the absence of microglia on debris clearance within lesions and to quantify vacuolization, we stained spinal cord sections with toluidine blue or LFB and hematoxylin and eosin (H&E at 21 dpi), a time when remyelination is ongoing in control mice. Sections stained with toluidine blue revealed extensive remyelination in control mice at 21 dpi as demonstrated by axons with thin myelin sheaths (Fig. 5*A*, arrowheads). However, in lesions of drug-treated mice, fewer axons were detected, and primarily unmyelinated axons and large vacuoles (Fig. 5*A*, arrows) were readily observed. Using the same LFB staining conditions shown in Fig. 2, we quantified the extent of damage within areas of demyelination and observed increased numbers and sizes of vacuoles within these lesions (Fig. 5 *B–D*, arrows). Furthermore, increased amounts of cellular debris, evidenced by fragmented

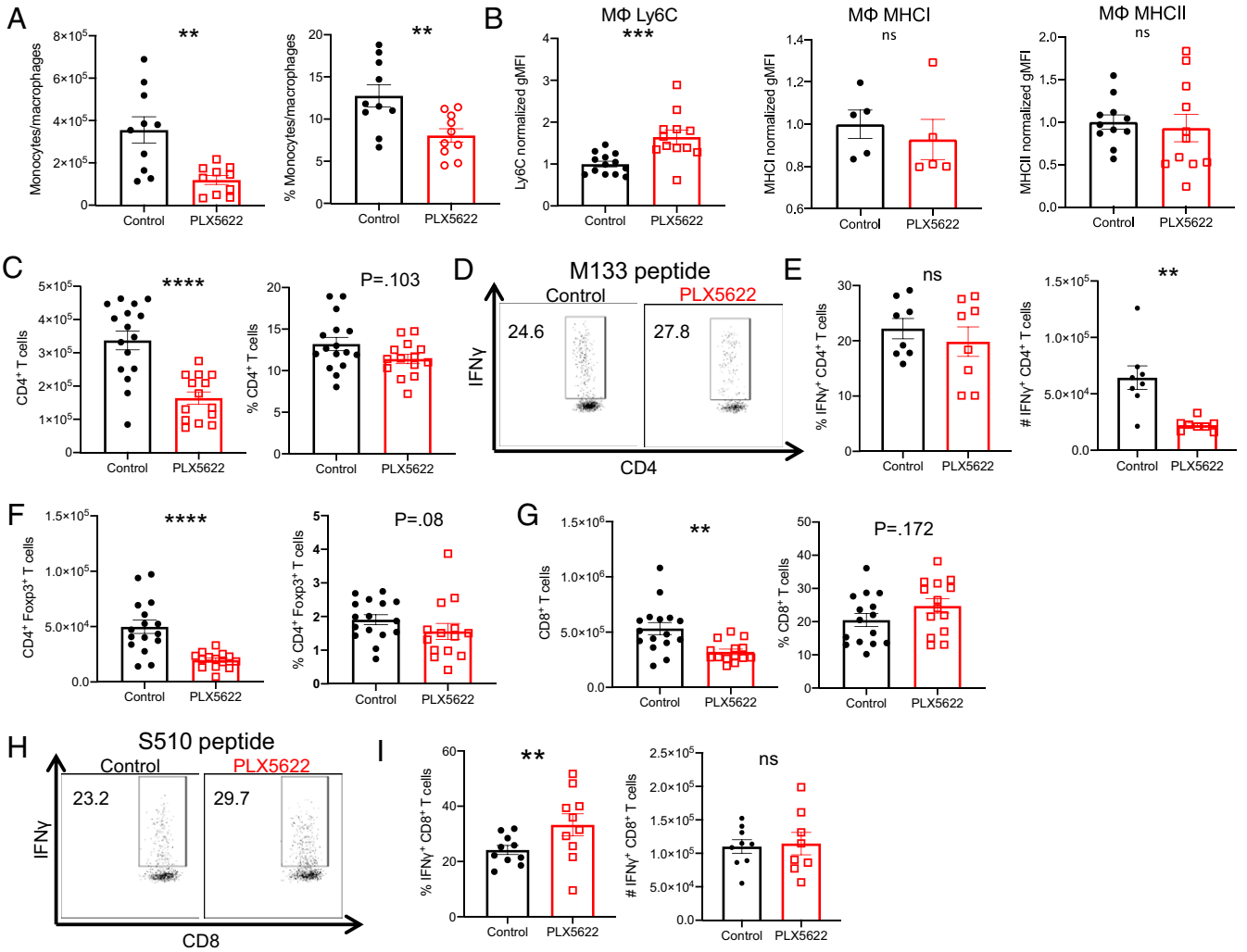

Fig. 3. Decreased immune infiltration in PLX5622-treated mice. Mice were infected and treated at 7 dpi as described above, and flow cytometry was used to analyze cells from the spinal cord at 14 dpi in PLX5622-treated and control mice. Number and frequency of monocytes/macrophages ($CD45^{hi}CD11b^{+}Ly6G^{-}$) (*A*), CD4 T cells (*C*), $Foxp3^{+}$ Tregs (*F*), and CD8 T cells (*G*). Normalized geometric MFI (gMFI) of Ly6C, MHCI, and MHCII staining in monocytes/macrophages (MΦ) (*B*). Virus-specific CD4+ T cell frequency and number were determined by IFN-γ intracellular cytokine staining (ICS) after stimulation with M133 peptide (*D* and *E*). Virus-specific CD8 T cell frequency and number were determined by IFN-γ ICS after stimulation with S510 peptide (*H* and *I*). Data represent combined results from two to three experiments with a combined total of 8–16 mice per group. Normalized gMFI (*B*) calculated as fold change over the mean of the control group for each experiment. Data represent the mean ± SEM, $^{**}P < 0.01$, $^{***}P < 0.001$, $^{****}P < 0.0001$ by Mann–Whitney *U* test.

and pyknotic (e.g., condensed chromatin) nuclear debris, was observed within these lesions, suggesting a defect in phagocytic function in the absence of microglia (Fig. 5*B*, arrowheads; Fig. 5*E*). Together, these results also indicate that, in the absence of microglia, infiltrating myeloid cells were unable to compensate for the role of microglia in clearing cellular debris from the lesion and creating a suitable environment for the recruitment of oligodendrocyte progenitor cells to the lesion or for their differentiation into myelinating oligodendrocytes.

Increased Myelin Debris in Demyelinating Lesions of Microglia-Depleted Mice. Since myelin debris presence is believed to inhibit remyelination, we next investigated myelin accumulation in the spinal cord at 21 dpi using electron microscopy (EM). Representative images of control (Fig. 6 *A–D*) and of drug-treated (Fig. 6 *E–H*) spinal cords are shown. Within areas of demyelination, more dystrophic axons were obvious in PLX5622-treated compared to control mice (Fig. 6 *A–C* and *E–H* arrows). Most remarkably, large amounts of vesiculated honeycomblike myelin debris were present in the drug-treated spinal cords, which were not observed in control spinal cords (Fig. 6 *E–G*, asterisks). Vesiculated myelin debris has been previously identified as closely associated with microglia or other phagocytic cells and is considered readily internalized (46, 47). However, in the absence of microglia, this myelin debris was largely observed in the absence of any obvious association with demyelinated axons or myeloid cells. In control mice, nucleated cells, probably microglia or infiltrating macrophages, were readily observed containing lamellar myelin debris and degenerating axons (Fig. 6 *A–C*, arrowheads, Fig. 6*D*, high magnification of the boxed region in Fig. 6*C*), emphasizing the key role that microglia rather than infiltrating macrophages play in myelin debris removal.

In order to further assess remyelination, g ratios, which are the ratios of inner axon diameter to the total myelinated axon diameter, were measured for axons in these electron micrographs of demyelinated regions. This allows for a measurement of myelination on a per-axon basis with lower ratios representing more myelination. Depletion of microglia resulted in a significantly increased g ratio relative to control mice (0.844–0.806, respectively), suggesting decreased remyelination (Fig. 7*A*). This further corroborates the reduced remyelination observed in Fig. 5*A*

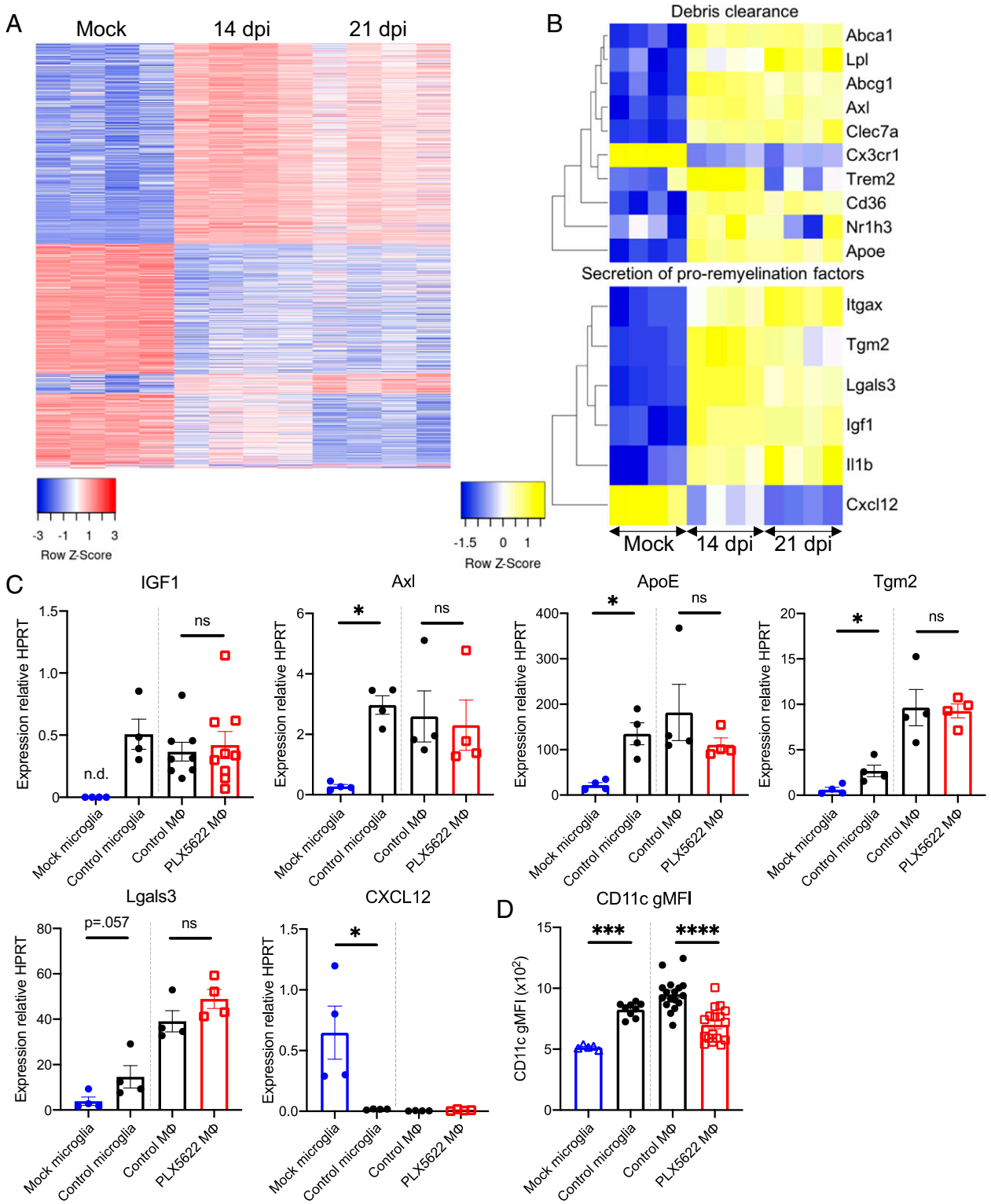

Fig. 4. Microglia express proremyelination and myelin debris removal genes. Microglia from mice at 14 and 21 dpi as well as mock-infected mice were isolated by a fluorescence-activated cell sorter for RNA-seq analysis. Heat maps show the 1,818 unique differentially expressed genes across each pairwise comparison (*A*) and selected genes involved in debris clearance and remyelination (*B*). Isolated microglia at 14 dpi and after mock infection and isolated monocytes/macrophages (MΦ) at 14 dpi from control- and PLX5622-treated mice were analyzed for the indicated mRNA transcripts by qPCR (*C*). Following infection and treatment with PLX5622-containing or control feed at 7 dpi, flow cytometry was used to analyze the geometric gMFI of CD11c in monocytes/macrophages at 14 dpi (*D*). Data in *A* and *B* were derived from four mice per group and analyzed as described in *Materials and Methods*. Data in *C* represent 4–9 mice per group. Data in *D* represent combined results from two to three experiments with a combined total of 5–17 mice per group. *n.d.*: undetermined Ct values. Data represent the mean ± SEM, $^{*}P < 0.05$, $^{***}P < 0.001$, $^{****}P < 0.0001$ by Mann–Whitney *U* test.

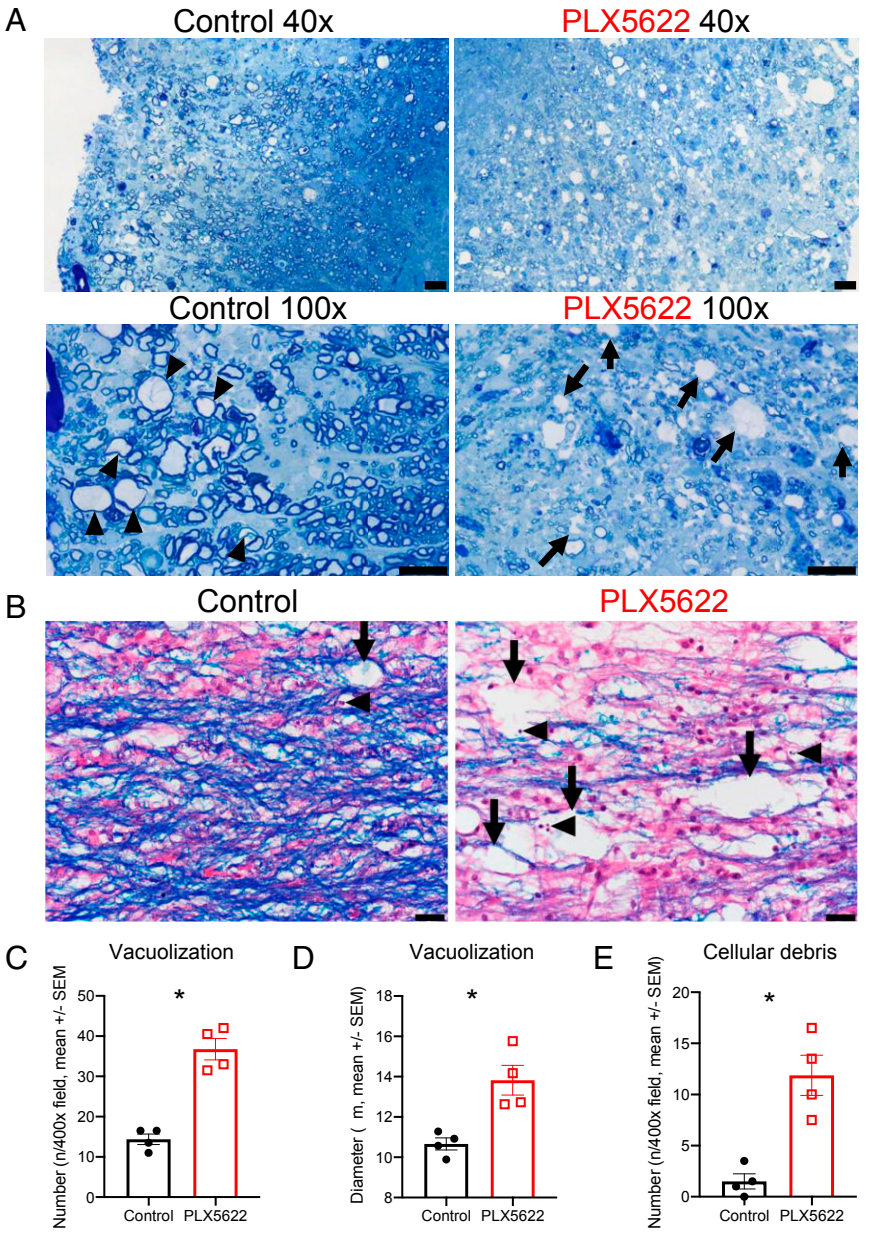

Fig. 5. Increased vacuolization and cellular debris in PLX5622-treated mice. Mice were infected and fed with PLX5622-containing or control chow starting at 7 dpi. Representative images of toluidine blue-stained spinal cords at 21 dpi (arrows: vacuoles; arrowheads: remyelinating axons) (*A*). Representative images of LFB-stained spinal cords at 21 dpi with vacuolization (arrows) and pyknotic nuclear debris (arrowheads) (*B*). Graphs show quantification of vacuole numbers (*C*) and size (*D*) as well as quantification of cellular debris (*E*). Images in *A* are representative of three mice per group. Images and quantification in *B–E* are representative of two fields per mouse and four mice per group (Scale bars, 20 μm.) Data represent the mean ± SEM, $*P < 0.05$ by Mann–Whitney *U* test.

and suggests a critical role for microglia in remyelination in this model.

Reduced Oligodendrocyte Numbers in Demyelinating Lesions of Microglia-Depleted Mice. To assess whether the absence of microglia resulted in a change in numbers of oligodendrocytes in the spinal cord, we quantified the number of $Olig2^+$ cells/mm^2 in the WM of mice at days 14 and 21 p.i. When we analyzed spinal cords at 21 dpi, we observed a twofold reduction in the number of oligodendrocytes in WM demyelinating lesions (WMLs) in PLX5622-treated mice compared to control mice (Fig. 8 *A* and *C*). The number of oligodendrocytes identified within lesions in PLX5622-treated mice was comparable to those observed in NAWM in control mice; too little NAWM was observed in drug-treated mice to allow quantification. We observed no significant differences in the numbers of $Olig2^+$ cells spinal cords at 14 dpi (Fig. 8*B*). Collectively, these results demonstrate that microglia are required for a limited time during the recovery phase and that part of their function is facilitating oligodendrocyte recruitment to lesions of demyelination.

Discussion

Here, we demonstrate that microglia play a critical protective role in promoting remyelination and ameliorating immune-mediated demyelination prior to 15 d p.i., which is the period of maximal myelin destruction. Analysis of PLX5622-treated mice demonstrated important roles for microglia in myelin and cellular debris removal and in promoting oligodendrocyte function. Most

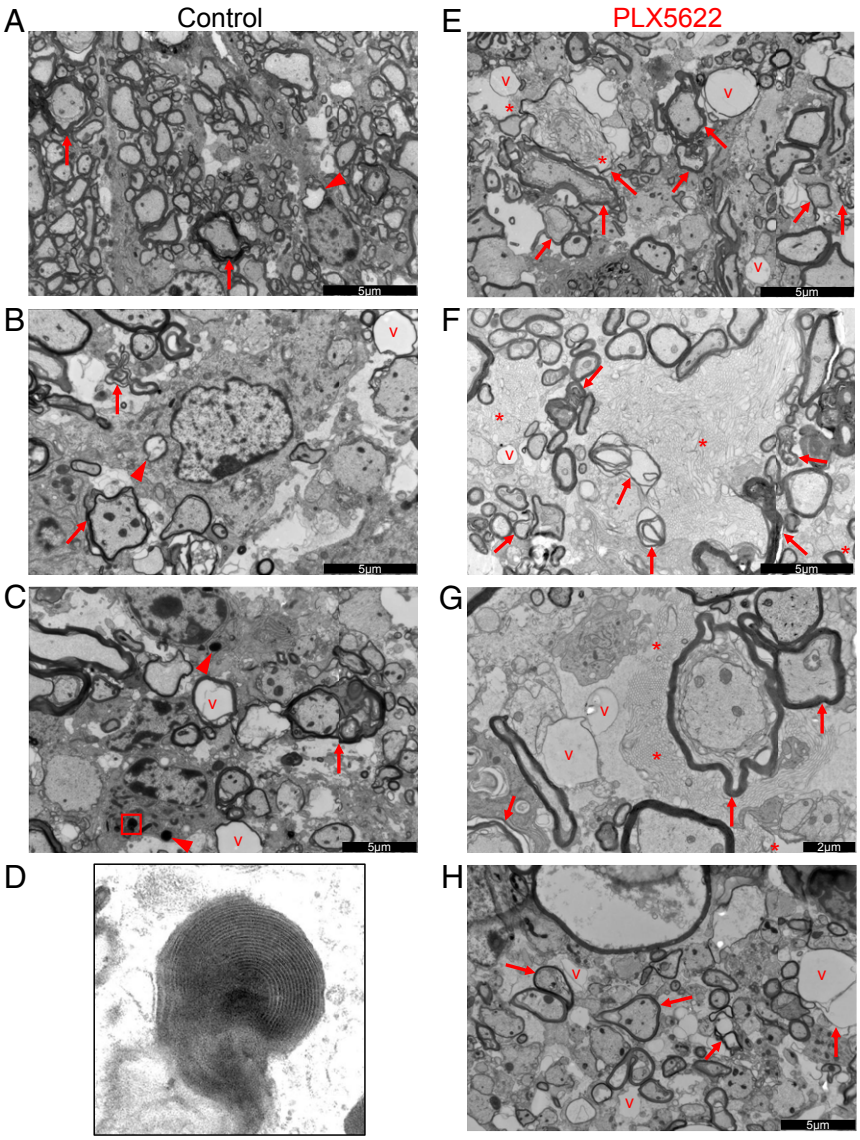

Fig. 6. Myelin debris clearance is impaired in PLX5622-treated mice. Mice were infected and fed with control (*A–D*) or PLX5622-containing (*E–H*) chow starting at 7 dpi. Shown are representative electron micrographs of spinal cord demyelinating lesions at 21 dpi with vacuolization (v), dystrophic, or degenerating axons (arrows), glial cells containing myelin or axonal inclusions (arrowheads), and vesiculated myelin debris (asterisks). Micrograph shown in *D* is a high magnification micrograph of the boxed region in *C*, demonstrating lamellar myelin debris within a glial cell. Micrographs are representative of three mice per group. Scale bars as indicated in the figure.

prominently, large deposits of extracellular myelin debris were evident in the spinal cords of PLX5622-treated mice and not in control mice, while phagocytosed myelin debris was detected in microglia and other cells to a much greater extent in control compared to drug-treated mice (Fig. 6). To provide quantification of the defect in phagocytosis and myelin damages, we assessed WM destruction and the presence of apoptotic debris in sections stained with LFB and identified significantly more debris and vacuolization in drug-treated mice. By EM, some of these vacuoles (Fig. 6, labeled "v") resemble "myelin balloons," which are fluid-containing myelin structures observed in aged animals and believed to result from degenerating axons (48). We also observed vacuoles that were not surrounded by myelin and may represent degenerating neuronal cell bodies or swollen dendrites (49).

Most striking in the EMs (Fig. 6 *E*, *F*, and *H*) were expansive regions of vesiculated myelin debris, that were not in apparent direct association with any specific axons, PLX5622-treated mice. This pattern of myelin degradation has previously been described in peripheral nerves of patients with lacquer thinner-induced neuropathy and in mice and primates with autoimmune demyelination (47, 50, 51). In general, vesiculated myelin debris in these studies is present in dystrophic axons and is associated with or present in phagocytic cells. In the absence of microglia, however, these large fields of debris are readily observed in the absence of nearby phagocytes, supporting a key role for microglia in debris clearance. Increased axon g ratios (Fig. 7*A*) additionally support the finding that the absence of microglia results in impaired remyelination as a lower ratio suggests more extensive myelination. These data are in agreement with a recent study of microglia depletion prior to MHV infection of the CNS (52).

These results also demonstrate the lack of redundancy of macrophages and microglia in the demyelinated CNS. While monocytes/macrophages were reduced in number in the CNS of PLX5622-treated mice (Fig. 3*A*), this was likely not due to direct

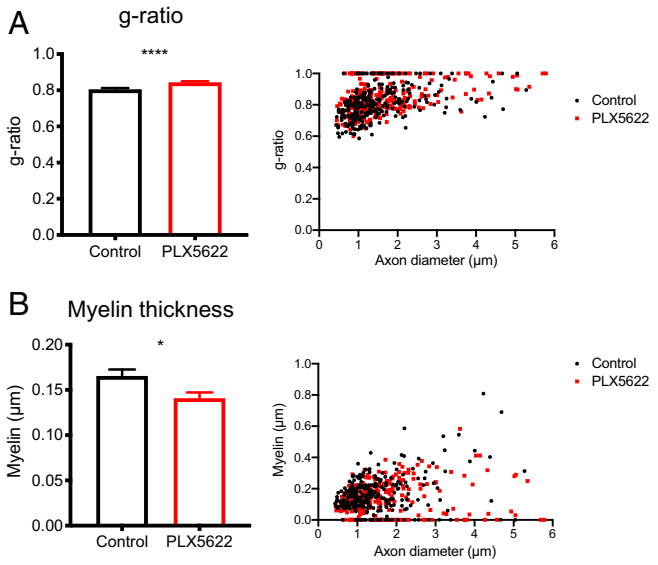

Fig. 7. Remyelination is impaired in PLX5622-treated mice. Infected mice were fed PLX5622-containing or control chow starting at 7 dpi. EMs of spinal cord demyelinating lesions were analyzed at 21 dpi. Calculation of the g ratio and scatter plot depicting the g ratio as a function of inner axon diameter (*A*). Myelin thickness and scatter plot depicting myelin thickness relative to inner axon diameter (*B*). $n = 265$ axons analyzed per group. Data represent the mean ± SEM, $^*P < 0.05$, $^{****}P < 0.0001$ by Mann–Whitney *U* test.

killing by the drug as previous studies using PLX5622-treated mice demonstrated little to no depletion of monocytes/macrophages in the periphery (23, 27). Furthermore, we observed increased numbers of these cells in the CNS if PLX5622 treatment was initiated prior to infection with JHMV (23). These results are consistent with others describing distinct functions for microglia and hematogenously derived macrophages in CNS pathologies (53–55). In one EAE study, macrophages were associated with demyelination, while microglia were anti-inflammatory and required for debris removal (53).

In addition to up-regulation of genes involved in clearance of myelin debris, our RNA sequencing analysis revealed that, at the peak of demyelination and during recovery, microglia up-regulate a number of factors described as proremyelinating, including those that have been proposed to promote oligodendrocyte maturation, proliferation, and localization (18, 38, 56). However, like the genes involved in myelin debris removal, microglial expression of these genes also appears to be required only for a limited period of time, prior to 15 d p.i. We show that numbers of Olig2+ cells at sites of demyelination at 21 dpi are decreased in PLX5622-treated spinal cords when compared to control spinal cords in which remyelination is partially or nearly completed. Notably, the numbers of Olig2+ cells in lesions in the drug-treated spinal cords were comparable to those in healthy WM from control mice. These results are consistent with the notion that oligodendrocyte progenitor cell migration into these sites of demyelination is diminished in the absence of microglia.

The role of microglia in CNS infection as well as other neuroinflammatory conditions appears variable, and these cells have been demonstrated to have a wide variety of roles in different disease contexts. During acute encephalitis caused by West Nile virus, TMEV, Dengue virus, Japanese encephalitis virus, pseudorabies virus, or MHV, depletion of microglia prior to infection uniformly resulted in worse outcomes with decreased kinetics of virus clearance and survival (23, 57–63). In mice that serve as a model for Alzheimer's disease, microglia depletion was generally beneficial by decreasing plaque formation (26). In the context of EAE or cuprizone-induced demyelination, microglia depletion resulted in enhanced or no change in remyelination, contrary to the results that we obtained in virus-induced demyelination (64, 65). However, other studies show that knockout of specific genes expressed by microglia in the demyelinated spinal cord contributed to suboptimal remyelination. Genetic deletion of proteins, such as Trem2 (66, 67), and those involved in cholesterol metabolism, such as Apolipoprotein E, Abca1, Abcg, and Lxra

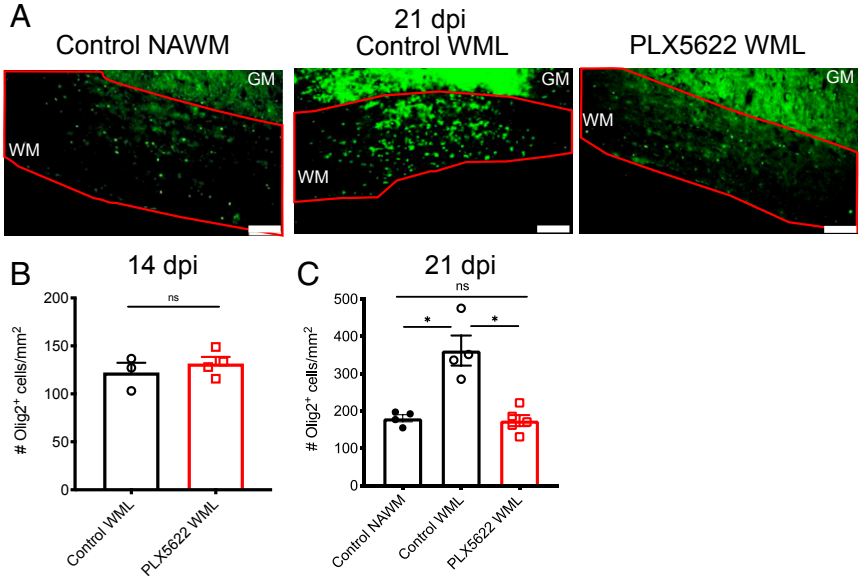

Fig. 8. Diminished oligodendrocyte accumulation in demyelinating lesions of PLX5622-treated mice. Infected mice were treated at day 7 p.i. with PLX5622-containing or control feed. Representative images of Olig2 immunostaining in normal appearing WM (NAWM) and WMLs of control-treated mice and WMsL of PLX5622-treated mice at 21 dpi, Scale bars, 100 μm. (*A*). Quantification of Olig2 staining in WMLs at 14 dpi (*B*) and in NAWMs and WMLs at 21 dpi (*C*). Too little NAWM was detected in drug-treated mice at day 21 p.i. to allow quantification. *GM*: gray matter; *WM*: white matter. Data in *B* are representative of three to four mice per group. Data in *C* show individual mice with four to five mice per group and represent the mean ± SEM, $^*P < 0.05$ by Mann–Whitney *U* test.

resulted in impaired myelin debris removal in vitro or in vivo (41). *Trem2* expression is additionally required for optimal expression of *Igf1* and remyelination (66). Microglia-specific deletion of lipoprotein lipase resulted in impaired debris uptake and exacerbated EAE (68). Collectively, these results indicate that microglia are essential for optimal myelin repair, although when microglia are completely absent in mice with autoimmune or chemically induced demyelination, their role is not as clear cut.

To summarize, our data, in conjunction with a previous report (23), indicate distinct roles for microglia in mice with a neurotropic coronavirus, facilitating early virus clearance and, then, later by enhancing myelin debris removal and enhancing oligodendrocyte accumulation at sites of demyelination. Given the variability with which patients recover from demyelinating disease, one explanation is that microglial dysfunction may contribute to both the tempo and the extent of remyelination.

Materials and Methods

Mice. Specific-pathogen-free C57BL/6 mice were purchased from Charles River Laboratories and maintained in a specific pathogen-free facility at the University of Iowa. Five- to seven-wk-old male mice were used in all experiments. Female mice exhibit similar clinical outcomes after JHMV infection, but results are less consistent. All animal studies were approved by the University of Iowa Animal Care and Use Committee and follow guidelines of the *Guide for the Care and Use of Laboratory Animals* (69).

Viral Infection and Clinical Scoring. All infections were performed using a recombinant version of the neuroattenuated J2.2-V-1 variant of JHMV (referred to as JHMV throughout) (22). JHMV is a neurotropic strain of MHV, a murine coronavirus. JHMV was propagated in 17Cl-1 cells (a murine fibroblast cell line) (70), and titers were determined using HeLa cells expressing the MHV receptor (HeLa-MHVR), CEACAM-1 (71). Five- to seven-week-old male mice were inoculated intracranially with 700 PFU of JHMV in 30 μL of Dulbecco's modified Eagle's medium (Gibco). Following inoculation, mice were monitored and weighed daily. Clinical scoring was based on the following criteria: 0, asymptomatic; 1, limp tail, mild hunching; 2, wobbly gait with mild righting difficulty, hunching; 3, hind-limb paresis and extreme righting difficulty; 4, hind-limb paralysis; 5, moribund.

PLX5622 Treatment. PLX5622 was provided by Plexxikon, Inc. AIN-76A rodent diet was formulated with 1,200 mg/kg PLX5622 by Research Diets. Mice were provided PLX5622-containing or standard AIN-76A chow beginning at 7 dpi through experimental endpoints unless otherwise specified.

Data Availability. Complete RNA-seq data were deposited in the NCBI's Gene Expression Omnibus (GEO) database, https://www.ncbi.nlm.nih.gov/geo/query/acc.cgi?acc (accession no. GSE144911).

Additional figures (*SI Appendix*, Figs. S1 and S2) supporting the main text are provided in the *SI Appendix*. A full overview of the methods, materials, and data referred to in this study is available in the *SI Appendix*.

ACKNOWLEDGMENTS. We thank Dr. Jian Zheng and Sunnie Hsiung for a critical review of the paper. Supported, in part, by Grants from the NIH (RO1 NS36592 [S.P.] and 2T32 GM067795 [A.S.]) and National Multiple Sclerosis Society (RG 5340-A-7). The authors acknowledge use of the University of Iowa Central Microscopy Research Facility and Flow Cytometry Facility, a core resource supported by the Vice President for Research & Economic Development and the Holden Comprehensive Cancer Center and the Carver College of Medicine.

1. E. O. Major, T. A. Yousry, D. B. Clifford, Pathogenesis of progressive multifocal leukoencephalopathy and risks associated with treatments for multiple sclerosis: A decade of lessons learned. *Lancet Neurol.* **17**, 467–480 (2018).
2. J. L. Soto-Hernandez, Human herpesvirus 6 encephalomyelitis. *Emerg. Infect. Dis.* **10**, 1700–1702 (2004).
3. S. Ozden, D. Seilhean, A. Gessain, J.-J. Hauw, O. Gout, Severe demyelinating myelopathy with low human T cell lymphotropic virus type 1 expression after transfusion in an immunosuppressed patient. *Clin. Infect. Dis.* **34**, 855–860 (2002).
4. W. W. Hall, P. W. Choppin, Measles-virus proteins in the brain tissue of patients with subacute sclerosing panencephalitis: Absence of the M protein. *N. Engl. J. Med.* **304**, 1152–1155 (1981).
5. E. Sundqvist *et al.*, Epstein-Barr virus and multiple sclerosis: Interaction with HLA. *Genes Immun.* **13**, 14–20 (2012).
6. C. Yea *et al.*; Canadian Pediatric Demyelinating Disease Network, Epstein-Barr virus in oral shedding of children with multiple sclerosis. *Neurology* **81**, 1392–1399 (2013).
7. J. D. Lünemann *et al.*, Elevated Epstein-Barr virus-encoded nuclear antigen-1 immune responses predict conversion to multiple sclerosis. *Ann. Neurol.* **67**, 159–169 (2010).
8. M. V. Tejada-Simon, Y. C. Q. Zang, J. Hong, V. M. Rivera, J. Z. Zhang, Cross-reactivity with myelin basic protein and human herpesvirus-6 in multiple sclerosis. *Ann. Neurol.* **53**, 189–197 (2003).
9. F. Ginhoux *et al.*, Fate mapping analysis reveals that adult microglia derive from primitive macrophages. *Science* **330**, 841–845 (2010).
10. U. Neniskyte, C. T. Gross, Errant gardeners: Glial-cell-dependent synaptic pruning and neurodevelopmental disorders. *Nat. Rev. Neurosci.* **18**, 658–670 (2017).
11. D. P. Schafer *et al.*, Microglia sculpt postnatal neural circuits in an activity and complement-dependent manner. *Neuron* **74**, 691–705 (2012).
12. A. Nimmerjahn, F. Kirchhoff, F. Helmchen, Resting microglial cells are highly dynamic surveillants of brain parenchyma in vivo. *Science* **308**, 1314–1318 (2005).
13. S. T. T. Schetters, D. Gomez-Nicola, J. J. Garcia-Vallejo, Y. Van Kooyk, Neuroinflammation: Microglia and T cells get ready to Tango. *Front. Immunol.* **8**, 1905 (2018).
14. C. Herzog *et al.*, Rapid clearance of cellular debris by microglia limits secondary neuronal cell death after brain injury in vivo. *Dev. Camb. Engl.* **146**, dev174698 (2019).
15. Z. Chen, D. Zhong, G. Li, The role of microglia in viral encephalitis: A review. *J. Neuroinflammation* **16**, 76 (2019).
16. S. Hickman, S. Izzy, P. Sen, L. Morsett, J. El Khoury, Microglia in neurodegeneration. *Nat. Neurosci.* **21**, 1359–1369 (2018).
17. S. Voet, M. Prinz, G. van Loo, Microglia in central nervous system inflammation and multiple sclerosis pathology. *Trends Mol. Med.* **25**, 112–123 (2019).
18. H. Neumann, M. R. Kotter, R. J. M. Franklin, Debris clearance by microglia: An essential link between degeneration and regeneration. *Brain* **132**, 288–295 (2009).
19. H. Solleiro-Villavicencio, S. Rivas-Arancibia, Effect of chronic oxidative stress on neuroinflammatory response mediated by $CD4^+T$ cells in neurodegenerative diseases. *Front. Cell. Neurosci.* **12**, 114 (2018).
20. C. C. Bergmann, T. E. Lane, S. A. Stohlman, Coronavirus infection of the central nervous system: Host-virus stand-off. *Nat. Rev. Microbiol.* **4**, 121–132 (2006).
21. A. E. Gorbalenya *et al.*; Coronaviridae Study Group of the International Committee on Taxonomy of Viruses, The species severe acute respiratory syndrome-related coronavirus: Classifying 2019-nCoV and naming it SARS-CoV-2. *Nat. Microbiol.* **5**, 536–544 (2020).
22. J. O. Fleming, M. D. Trousdale, F. A. el-Zaatari, S. A. Stohlman, L. P. Weiner, Pathogenicity of antigenic variants of murine coronavirus JHM selected with monoclonal antibodies. *J. Virol.* **58**, 869–875 (1986).
23. D. L. Wheeler, A. Sariol, D. K. Meyerholz, S. Perlman, Microglia are required for protection against lethal coronavirus encephalitis in mice. *J. Clin. Invest.* **128**, 931–943 (2018).
24. S. Xue, N. Sun, N. Van Rooijen, S. Perlman, Depletion of blood-borne macrophages does not reduce demyelination in mice infected with a neurotropic coronavirus. *J. Virol.* **73**, 6327–6334 (1999).
25. B. P. Chen, W. A. Kuziel, T. E. Lane, Lack of CCR2 results in increased mortality and impaired leukocyte activation and trafficking following infection of the central nervous system with a neurotropic coronavirus. *J. Immunol.* **167**, 4585–4592 (2001).
26. E. E. Spangenberg *et al.*, Eliminating microglia in Alzheimer's mice prevents neuronal loss without modulating amyloid-β pathology. *Brain* **139**, 1265–1281 (2016).
27. G. Szalay *et al.*, Microglia protect against brain injury and their selective elimination dysregulates neuronal network activity after stroke. *Nat. Commun.* **7**, 11499 (2016).
28. M. R. P. Elmore *et al.*, Colony-stimulating factor 1 receptor signaling is necessary for microglia viability, unmasking a microglia progenitor cell in the adult brain. *Neuron* **82**, 380–397 (2014).
29. L. Zhan *et al.*, Proximal recolonization by self-renewing microglia re-establishes microglial homeostasis in the adult mouse brain. *PLoS Biol.* **17**, e3000134 (2019).
30. G. F. Wu, A. A. Dandekar, L. Pewe, S. Perlman, CD4 and CD8 T cells have redundant but not identical roles in virus-induced demyelination. *J. Immunol.* **165**, 2278–2286 (2000).
31. F. I. Wang, S. A. Stohlman, J. O. Fleming, Demyelination induced by murine hepatitis virus JHM strain (MHV-4) is immunologically mediated. *J. Neuroimmunol.* **30**, 31–41 (1990).
32. J. J. Houtman, J. O. Fleming, Dissociation of demyelination and viral clearance in congenitally immunodeficient mice infected with murine coronavirus JHM. *J. Neurovirol.* **2**, 101–110 (1996).
33. S. Xue, A. Jaszewski, S. Perlman, Identification of a CD4+ T cell epitope within the M protein of a neurotropic coronavirus. *Virology* **208**, 173–179 (1995).
34. R. F. Castro, S. Perlman, CD8+ T-cell epitopes within the surface glycoprotein of a neurotropic coronavirus and correlation with pathogenicity. *J. Virol.* **69**, 8127–8131 (1995).
35. C. C. Bergmann, Q. Yao, M. Lin, S. A. Stohlman, The JHM strain of mouse hepatitis virus induces a spike protein-specific Db-restricted cytotoxic T cell response. *J. Gen. Virol.* **77**, 315–325 (1996).
36. M. Hlavica *et al.*, Intrathecal insulin-like growth factor 1 but not insulin enhances myelin repair in young and aged rats. *Neurosci. Lett.* **648**, 41–46 (2017).
37. A. Wlodarczyk *et al.*, A novel microglial subset plays a key role in myelinogenesis in developing brain. *EMBO J.* **36**, 3292–3308 (2017).
38. L. A. Pasquini *et al.*, Galectin-3 drives oligodendrocyte differentiation to control myelin integrity and function. *Cell Death Differ.* **18**, 1746–1756 (2011).
39. L. Thomas, L. A. Pasquini, Galectin-3-mediated glial crosstalk drives oligodendrocyte differentiation and (Re)myelination. *Front. Cell. Neurosci.* **12**, 297 (2018).

40. J. R. Patel, E. E. McCandless, D. Dorsey, R. S. Klein, CXCR4 promotes differentiation of oligodendrocyte progenitors and remyelination. *Proc. Natl. Acad. Sci. U.S.A.* **107**, 11062–11067 (2010).
41. L. Cantuti-Castelvetri *et al*., Defective cholesterol clearance limits remyelination in the aged central nervous system. *Science* **359**, 684–688 (2018).
42. M. Olah *et al*., Identification of a microglia phenotype supportive of remyelination. *Glia* **60**, 306–321 (2012).
43. J. G. Weinger *et al*., Loss of the receptor tyrosine kinase Axl leads to enhanced inflammation in the CNS and delayed removal of myelin debris during experimental autoimmune encephalomyelitis. *J. Neuroinflammation* **8**, 49 (2011).
44. A. Lampron *et al*., Inefficient clearance of myelin debris by microglia impairs remyelinating processes. *J. Exp. Med.* **212**, 481–495 (2015).
45. D. Nackiewicz *et al*., Islet macrophages shift to a reparative state following pancreatic beta-cell death and are a major source of islet insulin-like growth factor-1. *iScience* **23**, 100775 (2020).
46. W. W. Schlaepfer, Vesicular disruption of myelin simulated by exposure of nerve to calcium ionophore. *Nature* **265**, 734–736 (1977).
47. M. C. Dalcanto, H. M. Wiśniewski, A. B. Johnson, S. W. Brostoff, C. S. Raine, Vesicular disruption of myelin in autoimmune demyelination. *J. Neurol. Sci.* **24**, 313–319 (1975).
48. A. Peters, The effects of normal aging on myelin and nerve fibers: A review. *J. Neurocytol.* **31**, 581–593 (2002).
49. J. Das Sarma, L. C. Kenyon, S. T. Hingley, K. S. Shindler, Mechanisms of primary axonal damage in a viral model of multiple sclerosis. *J. Neurosci.* **29**, 10272–10280 (2009).
50. M.-T. Weil *et al*., Loss of myelin basic protein function triggers myelin breakdown in models of demyelinating diseases. *Cell Rep.* **16**, 314–322 (2016).
51. P. W. Lampert, Demyelination and remyelination in experimental allergic Encephalomyelitis: Further electron microscopic observations. *J. Neuropathol. Exp. Neurol.* **24**, 371–385 (1965).
52. V. Mangale *et al*., Microglia influence host defense, disease, and repair following murine coronavirus infection of the central nervous system. *Glia*, 10.1002/glia.23844 (2020).
53. R. Yamasaki *et al*., Differential roles of microglia and monocytes in the inflamed central nervous system. *J. Exp. Med.* **211**, 1533–1549 (2014).
54. A. London, M. Cohen, M. Schwartz, Microglia and monocyte-derived macrophages: Functionally distinct populations that act in concert in CNS plasticity and repair. *Front. Cell. Neurosci.* **7**, 34 (2013).
55. G. Kronenberg *et al*., Distinguishing features of microglia- and monocyte-derived macrophages after stroke. *Acta Neuropathol.* **135**, 551–568 (2018).
56. J. L. Mason *et al*., Mature oligodendrocyte apoptosis precedes IGF-1 production and oligodendrocyte progenitor accumulation and differentiation during demyelination/remyelination. *J. Neurosci. Res.* **61**, 251–262 (2000).
57. K. E. Funk, R. S. Klein, CSF1R antagonism limits local restimulation of antiviral $CD8^+$ T cells during viral encephalitis. *J. Neuroinflammation* **16**, 22 (2019).
58. J. M. S. Sanchez *et al*., Microglial cell depletion is fatal with low level picornavirus infection of the central nervous system. *J. Neurovirol.* **25**, 415–421 (2019).
59. A. B. DePaula-Silva *et al*., Differential transcriptional profiles identify microglial- and macrophage-specific gene markers expressed during virus-induced neuroinflammation. *J. Neuroinflammation* **16**, 152 (2019).
60. T.-T. Tsai *et al*., Microglia retard dengue virus-induced acute viral encephalitis. *Sci. Rep.* **6**, 27670 (2016).
61. S. Seitz, P. Clarke, K. L. Tyler, Pharmacologic depletion of microglia increases viral load in the brain and enhances mortality in murine models of flavivirus-induced encephalitis. *J. Virol.* **92**, e00525-18 (2018).
62. R. Fekete *et al*., Microglia control the spread of neurotropic virus infection via P2Y12 signalling and recruit monocytes through P2Y12-independent mechanisms. *Acta Neuropathol.* **136**, 461–482 (2018).
63. D. G. Brown *et al*., The microbiota protects from viral-induced neurologic damage through microglia-intrinsic TLR signaling. *eLife* **8**, e47117 (2019).
64. J. C. Nissen, K. K. Thompson, B. L. West, S. E. Tsirka, Csf1R inhibition attenuates experimental autoimmune encephalomyelitis and promotes recovery. *Exp. Neurol.* **307**, 24–36 (2018).
65. N. Beckmann *et al*., Brain region-specific enhancement of remyelination and prevention of demyelination by the CSF1R kinase inhibitor BLZ945. *Acta Neuropathol. Commun.* **6**, 9 (2018).
66. P. L. Poliani *et al*., TREM2 sustains microglial expansion during aging and response to demyelination. *J. Clin. Invest.* **125**, 2161–2170 (2015).
67. C. Cantoni *et al*., TREM2 regulates microglial cell activation in response to demyelination in vivo. *Acta Neuropathol.* **129**, 429–447 (2015).
68. K. D. Bruce *et al*., Lipoprotein lipase is a feature of alternatively-activated microglia and may facilitate lipid uptake in the CNS during demyelination. *Front. Mol. Neurosci.* **11**, 57 (2018).
69. National Research Council, *Guide for the Care and Use of Laboratory Animals*, (National Academies Press, Washington, DC, ed. 8, 2011).
70. S. Perlman, D. Ries, E. Bolger, L. J. Chang, C. M. Stoltzfus, MHV nucleocapsid synthesis in the presence of cycloheximide and accumulation of negative strand MHV RNA. *Virus Res.* **6**, 261–272 (1986).
71. R. K. Williams, G. S. Jiang, K. V. Holmes, Receptor for mouse hepatitis virus is a member of the carcinoembryonic antigen family of glycoproteins. *Proc. Natl. Acad. Sci. U.S.A.* **88**, 5533–5536 (1991).